Applied Catalysis B: Environmental 328 (2023) 122544

Contents lists available at ScienceDirect

Applied Catalysis B: Environmental

journal homepage: www.elsevier.com/locate/apcatb

Efficient and highly selective direct electrochemical oxidation of ammonia to dinitrogen facilitated by NiCu diatomic site catalysts

Huimin Zhang [a,*], Hailong Wang [a], Luanqi Zhou [a], Qiming Li [a], Xu Yang [b], Yifei Wang [c], Meng Zhang [d], Zucheng Wu [b]

[a] School of Civil Engineering and Architecture, East China Jiao Tong University, Nanchang, Jiangxi 330013, China
[b] Department of Environmental Engineering, Laboratory of Electrochemistry and Energy Storage, State Key Laboratory of Clean Energy Utilization, Zhejiang University, Hangzhou 310058, China
[c] School of Mechanical Engineering and Automation, Harbin Institute of Technology, Shenzhen, China
[d] Jiangxi Academy of Eco-environmental Sciences and Planning, Nanchang, Jiangxi 330039, China

ARTICLE INFO

Keywords:
Ammonia-nitrogen removal
Direct electrochemical oxidation
AOR
$NiCu_3$-N-C DAC
N_2 selectivity

ABSTRACT

Direct electrochemical oxidation has recently received increasing attention in ammonia-nitrogen wastewater treatment. However, how to catalyze the oxidation of ammonia to N_2 with high selectivity retains a tremendous challenge. In this work, $NiCu_3$-N-C diatomic site catalyst (DAC) anchored in nitrogen-doped carbon was synthesized via solid-phase pyrolysis. HAADF-STEM and XAFS characterizations demonstrated the high dispersion of adjacent Ni/Cu diatomic sites and the micro-environment of Ni-N_4/Cu-N_4 groups. The experiment results exhibit that $NiCu_3$-N-C DAC has an eminent intrinsic activity towards AOR with a *TOF* of 3.64 s^{-1} at 1.50 V vs. RHE. Consequently, in a real wastewater with 616 mg/L NH_4^+-N, 99.52% of removal efficiency and 86.60% of faradaic efficiency (*FE*) after a 6-hour degradation experiment were acquired with a high N_2 selectivity of 97.87%, confirming its excellent catalytic performance. This work furnishes a good example of rationally designing functionally coordinated diatomic site catalysts (DACs) for the efficient treatment of ammonia-nitrogen wastewater.

1. Introduction

Nowadays, the global imbalance in the nitrogen cycle is becoming increasingly serious due to the growing indiscriminate discharge of nitrogenous pollutants[1,2]. Ammonia-nitrogen (NH_4^+-N) mainly originates from domestic sewage, industrial wastewater, and farmland drainage, which can lead to a range of environmental problems, such as eutrophication and black odor in water bodies[3,4]. Compared with conventional processing technologies such as biological treatment[5,6], breakpoint chlorination[7] and air stripping[8], electrochemical oxidation technology has the merits of simple operation, cost-effectiveness and good tolerance to toxic pollutants as a promising candidate[9–11]. Generally, indirect electrochemical oxidation refers to the rapid oxidation of ammonia by means of chlorine radicals (Cl·, ClO·, etc.), which requires large amounts of chlorine salts and easily produces toxic chlorinated by-products[12,13]. Direct electrochemical oxidation is the direct catalytic oxidation of ammonia to N_2 under the intervention of catalyst, which is more environmentally friendly and economical. The reaction for direct electrochemical oxidation of ammonia is as follows [14]:

$$\text{Anodic}: \ NH_3(aq) + 3OH^- \rightarrow 1/2N_2\uparrow + 3H_2O + 3e^- \ E^0 = -0.77 \text{ V vs. SHE} \quad (1)$$

$$\text{Cathodic}: \ 3H_2O + 3e^- \rightarrow 3/2H_2\uparrow + 3OH^- \ E^0 = -0.83 \text{ V vs. SHE} \quad (2)$$

$$\text{Overall}: \ NH_3(aq) \rightarrow 1/2N_2\uparrow + 3/2H_2\uparrow \ \Delta E^0 = 0.06 \text{ V vs. SHE} \quad (3)$$

However, due to the strong N-H bond (99.5 kcal/mol) in the ammonia molecule, direct electrochemical ammonia oxidation reaction (AOR) usually faces with large overpotential and kinetic hysteresis[15,16]. To date, many catalysts constructed from noble metals (e.g., Pt, Ir and Pd)[17,18], transition metals (Ni and Cu, etc.)[19,20], or their alloys [21–27] have been reported aiming to efficiently catalyze AOR. Nevertheless, the catalysts mostly exist in the form of nanoparticles, whose internal active centers are not fully utilized, bringing redundancy and partial loss of overall catalytic activity[28,29]. In addition, the

* Corresponding author.
E-mail address: zhanghm@zju.edu.cn (H. Zhang).

https://doi.org/10.1016/j.apcatb.2023.122544
Received 22 November 2022; Received in revised form 14 January 2023; Accepted 26 February 2023
Available online 28 February 2023

diverse expression of active centers on nano- and larger-sized catalysts during direct electrochemical oxidation easily leads to the peroxidation of ammonia. It can accumulate massive by-products such as NO_2^- and NO_3^- during short running period, which were unwanted secondary pollutants in the environment[30,31]. To address these issues, it is imperative to design and exploit a stable and efficient catalyst for the highly selective direct electrochemical oxidation of ammonia to the desired product, dinitrogen.

Single atom catalysts (SACs), which possess fully disclosed and explicit active centers, have recently shown dramatic potential in the fields of CO_2 reduction reactions (CO_2RR)[32,33], oxygen evolution reactions (OER)[34] and nitrogen reduction reactions (NRR)[35,36]. The performance of SACs is inextricably linked to the loading, micro-environment of the central metal and the surface state of the carrier[37,38]. Among them, atomic metal-nitrogen (M-N_4, M = Ni, Fe, Co, etc.) materials anchored in porous carbon backbones are particularly prominent in these fields[39]. M-N_4 species have N-coordination metal centers, which is like natural metalloporphyrin and has good thermal and chemical stability[40,41]. However, due to the inherent electronic structure of the catalyst and the insufficient flexibility of the single atomic site, it is difficult to balance the adsorption energy of various reaction intermediates, hindering the optimization of catalytic activity and product selectivity to a certain extent[42]. In order to further optimize and improve the catalytic performance of atomic catalysts, diatomic sites catalysts (DACs) with significantly different functional coordination and confinement effects were proposed and applied[43]. Take a CO_2RR work as an example, the single metal site Ni-N_4 or Fe-N_4 is hard to equilibrate the adsorption free energy of intermediates CO* and COOH* , whose catalytic utility and selectivity are significantly inferior to those of the bimetallic sites Ni-N_4/Fe-N_4[44]. The introduction of the second metal site brings the electron coupling effect between metals, optimizing the electronic structure of the catalysts and ameliorating the adsorption balance of various intermediates. Also, it provides more top/bridge sites for the reaction, thereby greatly enhancing the CO_2RR activity and selectivity[45]. In many reports such as NiCu[46,47], FeCo [48], NiCo[49] and NiIr[50], the unique advantages and effective applications of DACs have been highlighted in reducing the overpotential and accelerating the reaction kinetics of multi-step electrocatalytic reactions (CO_2RR, OER, ORR and etc.). Nevertheless, to the best of our knowledge, there are few reports about the application of DACs in electrocatalytic AOR.

Herein, we designed a $NiCu_3$-N-C DAC immobilized on a nitrogen-doped porous carbon via solid-phase pyrolysis method, which can catalyze AOR efficiently and selectively. The adjacent Ni-N_4/Cu-N_4 diatomic site structure of the catalyst was uncovered drawing from high angle annular dark field scanning transmission electron microscopy (HAADF-STEM) and X-ray absorption fine spectroscopy (XAFS). The experiment results confirm that the excellent electronic coupling effect between the bimetallic sites can optimize the internal electronic structure in catalyst, obtaining an onset potential significantly lower than Ni-N-C or Cu-N-C. Consequently, $NiCu_3$-N-C DAC facilitates electrocatalytic AOR, exhibiting an excellent removal efficiency and N_2 selectivity. Overall, Ni-N_4/Cu-N_4 diatomic sites in $NiCu_3$-N-C DAC can achieve the desired pathway for AOR, advancing the development of direct electrochemical oxidation technology in ammonia-nitrogen wastewater treatment.

2. Experimental section

2.1. Synthesis of $NiCu_3$-N-C DAC

At first, 10 g of trisodium citrate was transferred to a muffle furnace with a quartz crucible device and pyrolyzed at a constant temperature of 800 ℃ under N_2 atmosphere for 1 h. The obtained product was rinsed sequentially using sulfuric acid solution (1.0 M) and deionized water (18.2 MΩ), thereby eliminating inorganic impurities. The porous carbon (PC) support was acquired after drying at 80 ℃. Whereupon, PC (60 mg), $NiSO_4{\cdot}7\ H_2O$ (0.3 mmol), $CuSO_4{\cdot}5\ H_2O$ (1.2 mmol) and glucose (6 mmol) were mixed and ground into uniform powder. After drying at 60 ℃ for 30 min, the sample was weighed and recorded as M_1. Melamine with a mass of 5 times that of M_1 was added, then mixed and ground into a uniform fine powder. Then, it was pyrolyzed for 2 h at 800 ℃ in the muffle furnace, which is filled with a N_2 atmosphere. The obtained powder was taken out after cooling, grinded and screened to gain the sample of $NiCu_3$-N-C DAC. In addition, the control catalysts were obtained by the same method, respectively described as Ni-N-C, NiCu-N-C, $NiCu_2$-N-C, $NiCu_4$-N-C and Cu-N-C (Where, the subscript is the initial stoichiometric ratio of the metal salt in the precursor, Cu/Ni). The loading of the catalysts on the CP substrate was controlled to 1.5 mg/cm^2 for each electrochemical measurement.

2.2. The treatment of ammonia-nitrogen wastewater

The ammonia-nitrogen removal experiments of synthetic wastewater were performed in a three-electrode system for 5 h under different conditions. Firstly, the removal efficiency of NH_4^+-N and its product selectivity were probed on the $NiCu_3$-N-C DAC electrode under different initial concentrations of NH_4^+-N (i.e., 350, 700 and 1400 mg/L). Then, the effect of different operating potentials on the utilization efficiency of the $NiCu_3$-N-C DAC was analyzed, including 1.60 V, 1.55 V, 1.50 V, 1.45 V and 1.40 V vs. RHE. Also, the experiment was proceeded for control catalysts under the optimal condition obtained from that on $NiCu_3$-N-C DAC. To further examine the practicality of $NiCu_3$-N-C DAC, the ammonia-nitrogen removal experiment of real wastewater at the optimal condition were carried out. Finally, the experiment using real wastewater was carried out for prepared nanoscale Ni_1Cu_3-S-T/CP and $Ni_1Cu_1Co_{0.5}$-S-T/CP catalysts as a comparison (See supporting documents for more experimental details). Wherein, the synthetic wastewater refers to the ammonia solution with the initial NH_4^+-N concentration of C_0 (equal to 350, 700 or 1400 mg/L) and 0.25 M NaOH. The real wastewater was composed of 0.25 M NaOH and a landfill leachate containing 616 mg/L NH_4^+-N, with 150 mg/L NO_3^--N and 305 mg/L NO_2^--N.

3. Results and discussions

3.1. Physical characterization

The synthesis process of $NiCu_3$-N-C DAC is shown in Fig. 1. PC, nitrogen source, Ni and Cu precursors were mixed and ground homogeneously, followed by one-step high-temperature pyrolysis at 800 °C. Then, $NiCu_3$-N-C DAC was obtained, where NiN_4-CuN_4 diatomic site structure was anchored in a porous carbon skeleton with two adjacent isolated CuN_4 structures. HRTEM images displayed that no large metal particles were found as shown in Fig. 2a. Notably, the catalyst surface is

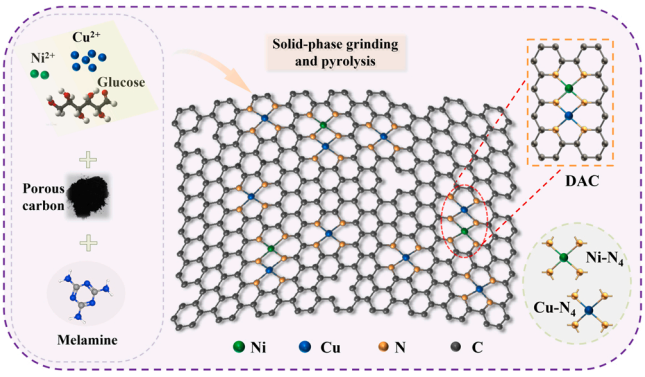

Fig. 1. Schematic diagram of $NiCu_3$-N-C DAC fabrication.

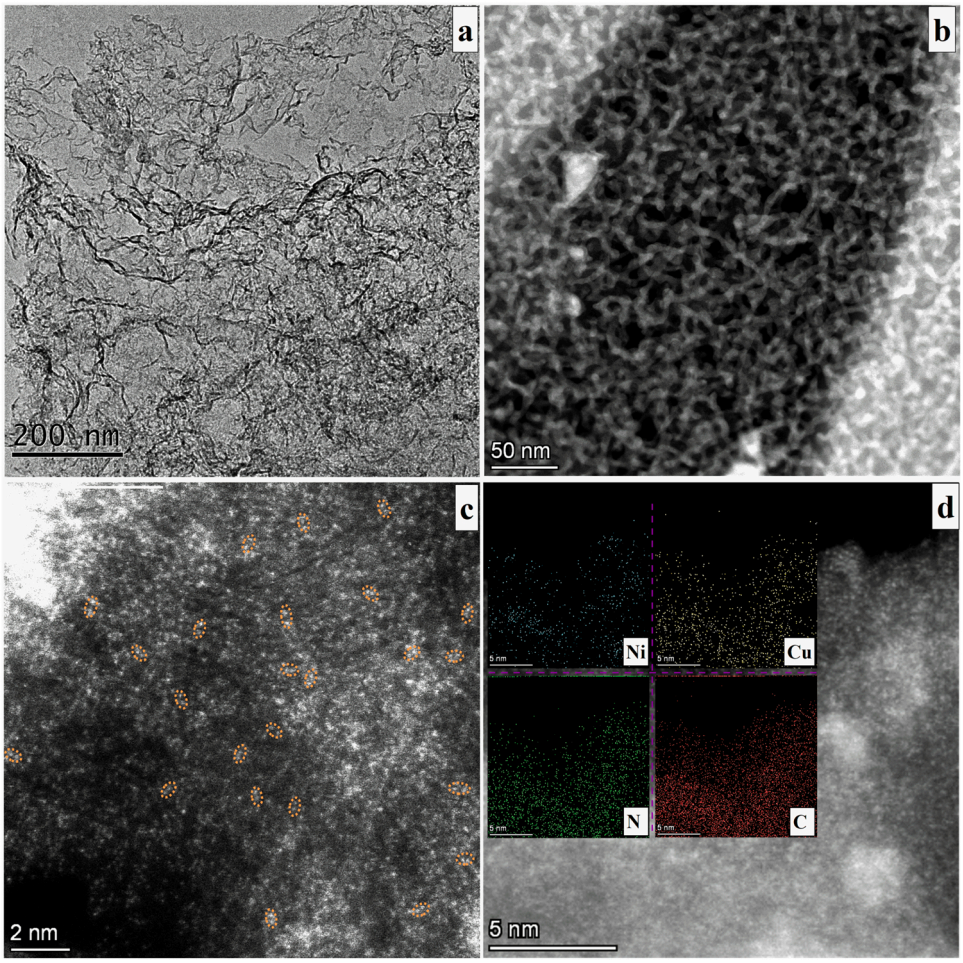

Fig. 2. (a) HRTEM image; (b) HAADF-STEM image; (c) Enlarged HAADF-STEM image; (d) EDS mapping, all collected on $NiCu_3$-N-C DAC.

overlaid by a flocculent structure, which is classic for pyrolysis carbonaceous materials (e.g., dextrose). Clearly, HAADF-STEM characterization displays that the nitrogen-doped carbon substrate has a three-dimensional porous skeleton morphology, which provides a good anchor site for immobilizing the active metal center (Fig. 2b and S1). As shown in Fig. 2c, large amounts of bright spots associated with Ni/Cu atoms were clearly observed, revealing the dense distribution of isolated atoms. Interestingly, except for isolated monatoms, the circled bright spots around them demonstrate the presence of adjacent metal sites, which is consistent with the previously reported diatomic structure[51, 52]. EDS energy spectrum proves the existence of Ni, Cu, N and C elements, and the corresponding element mapping displays the uniform element distribution and no presense of large aggregates (Fig. 2d and S2). Moreover, the atomic contents of Ni and Cu in $NiCu_3$-N-C DAC are 4.773 wt% and 13.241 wt% (Table S1), respectively, determined by ICP-OES. The measured Cu/Ni ratio is basically consistent with the initial stoichiometric ratio.

The XRD pattern (Fig. 3a) displays that $NiCu_3$-N-C, Ni-N-C and Cu-N-C samples all present alike diffraction patterns with a broad peak of carbon at 26.309° (Carbon, PDF#75–0444). On the sample surface, some diffraction peaks belonging to the nickel (PDF#89–7128) and copper (PDF#89–2838) were observed, but were extremely weak. It indicates that no Ni/Cu nanoparticles or clusters were formed. Subsequently, the valence bond composition of the catalyst was characterized by XPS spectra. In the C 1 s spectrum of the sample, the four peaks of C-C (284.8 eV), C-N (286.3 eV), C═N (287.9 eV) and C═O (289.9 eV) bonds were observed, evidencing the succeeded doping of N into the carbon skeleton (Fig. 3b). The N 1 s spectrum indicated two peaks at 397.5 eV and 401.8 eV, which can be individually assigned to pyridinic and graphitic species (Fig. 3c). In particular, another characteristic peak represents porphyrin-like fractions at 399.6 eV, which belongs to the coordination of metal-nitrogen (M-N)[44,53]. Besides, the full spectrum, Ni 2p and Cu 2p XPS spectra of $NiCu_3$-N-C were illustrated in Fig. S3. It is evident that there are three spectral peaks at 854.2, 856.0 and 871.4 eV, which can be assigned mainly to Ni(I), and possibly Ni(0) and Ni(II). Similarly, four spectral peaks appear at 931.6, 933.3, 951.6 and 954.8 eV in the Cu 2p spectrum, which are well matched with Cu(I) or Cu(II). Then, combined with the results of XANES spectra, the oxidation states of Ni and Cu in the catalyst are concluded to be + 1. These display that Ni and Cu atoms are well anchored in N-doped porous carbon carriers.

Furthermore, the micro-environment structure and electronic properties of $NiCu_3$-N-C DAC were unveiled by XANES and EXAFS. In the Ni K-edge XANES spectrum (Fig. 4a), the near-edge absorption energy of the $NiCu_3$-N-C sample is intermediate between that of Ni-Foil and NiO, indicating that the valence state of nickel is in the range of 0 to + 2. Similarly, the Cu K-edge XANES spectrum indicates that its near-edge absorption energy is between Cu-Foil and CuO and almost overlapped with Cu_2O, which means that the chemical state of Cu is close-by the + 1 valence (Fig. 4b). As seen in Fourier transform (FT) k^3-weighted EXAFS spectra, the primary peak of the sample is located at 1.45 Å compared to standard nickel phthalocyanine (Ni-Pc), indicating the predominant postion of Ni-N coordination (Fig. 4c). Similarly, referring to the standard copper phthalocyanine (Cu-Pc), the dominant peak of the sample at 1.4 Å was correlated with Cu-N bonding (Fig. 4d). It is of interest to note that the main peak of the sample has a certain shift compared with the

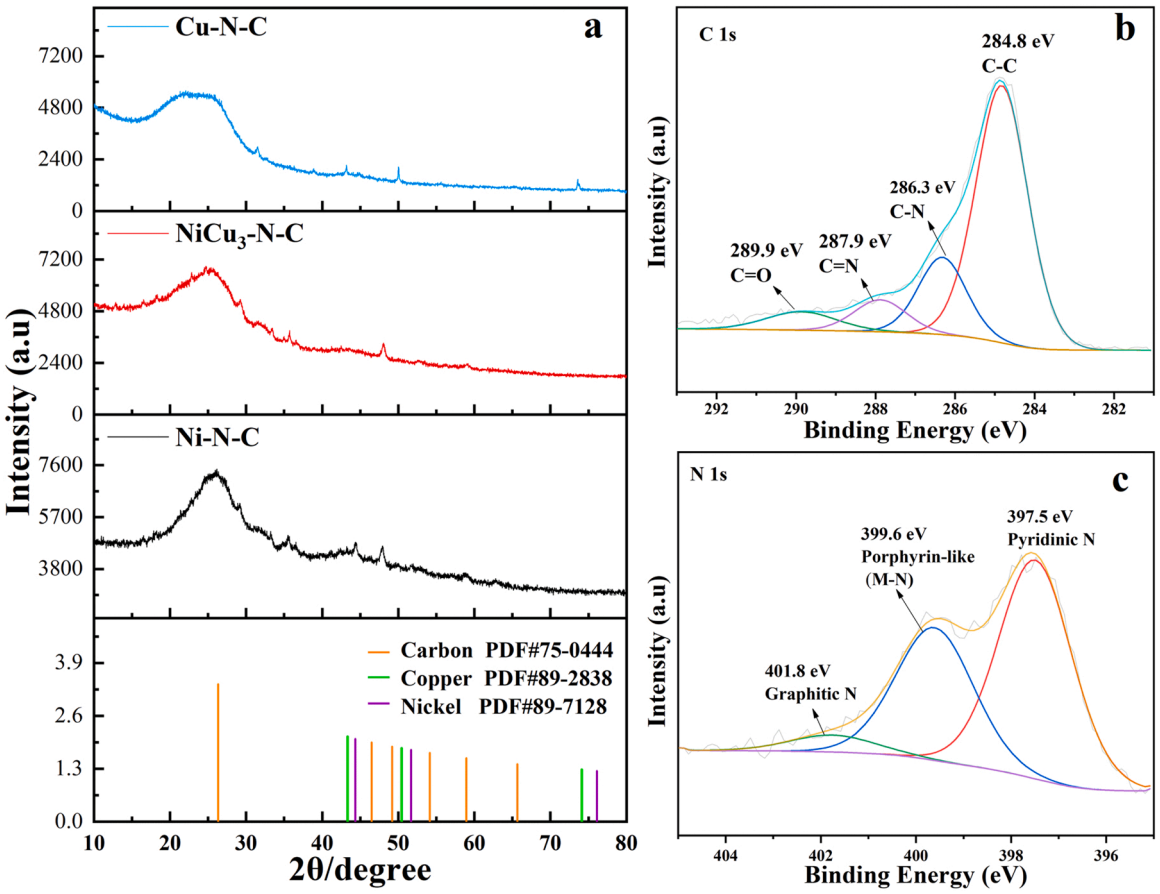

Fig. 3. (a) XRD patterns of Ni-N-C, $NiCu_3$-N-C and Cu-N-C; (b) C 1s and (c) N 1s XPS spectra of $NiCu_3$-N-C.

two standard phthalocyanines. This indicates that there is electronic interaction in the diatomic active center and the spatial characteristics of charge redistribution induced by nitrogen doping. The metals coordination characteristics of Ni-Ni (2.15 Å) and Cu-Cu (2.25 Å) were not observed, which confirmed the absence of metal nanoparticles or clusters. That is to say, Ni and Cu in $NiCu_3$-N-C DAC are atomically distributed on the carbon skeleton in cooperation with the metal-nitrogen coordination bonds.

Meanwhile, wavelet transform (WT) plots that provide *k* and R spatial resolution are used for corroborating the aforementioned deduction. In Fig. 4f, the WT isoline map of $NiCu_3$-N-C DAC represents an intense signal response of 4.5 $Å^{-1}$, which is similar to the characteristic of Ni-Pc (4.3 $Å^{-1}$), owing to the contribution of Ni-N. In contrast to Ni-foil (8.5 $Å^{-1}$), there is no Ni-Ni signal observed, which can further rule out the existence of Ni nanoparticles. Similarly, the intense signal response in the WT isoline map of $NiCu_3$-N-C DAC is close to that of Cu-Pc (4.4 $Å^{-1}$), which is attributed to the contribution of Cu-N (Fig. S8). Note that no Cu-Cu signal similar to that in Cu foil (8.2 $Å^{-1}$) is observed, then the presence of Cu nanoparticles can be excluded. As acquired via the fitting results of Ni K-edge EXAFS, the Ni-N coordination number is 4.2 (Fig. 4e and Table S2). Also, the Cu-N coordination number of 4.5 is determined by the fitting results of Cu K-edge EXAFS (Fig. S4 and Table S3). In brief, the local coordination environment at the Ni/Cu diatomic sites of $NiCu_3$-N-C DAC was confirmed as a $Ni\text{-}N_4/Cu\text{-}N_4$ structure. Isolated nickel/copper atom interactions in adjacent metal-nitrogen coordination can lead to the change of the internal electronic structure in the catalyst.

3.2. Electrochemical performance of the catalysts

Electrochemical tests, such as LSV, EIS, were conducted in the ammonia electrolyte to evaluate the electrochemical performance of various catalysts. Fig. 5a shows that with the increase of Cu/Ni ratio, the AOR current density first raised and then dropped. Among them, $NiCu_3$-N-C DAC reached a high current density of 88.58 mA/cm^2 @ 1.69 V vs. RHE, nearly 12 times higher than Ni-N-C (7.23 mA/cm^2). Interestingly, the onset potential @ 5 mA/cm^2 of AOR on the catalysts surface was also regulated by the Cu/Ni ratio. $NiCu_3$-N-C DAC obtained the lowest onset potential (1.203 V), which was negatively shifted by 0.413 V and 0.306 V compared to Ni-N-C SAC and Cu-N-C SAC, separately (Table S4). The coordination of Ni/Cu diatoms significantly accelerates the kinetics of the reaction, driving AOR to start early at a lower potential. Perhaps it stems from the fact that the electron interaction between nickel and copper diatoms is optimal at the Cu/Ni ratio of 3/1.

Turnover frequency (*TOF*) is applied to reflect the inherent activity of the catalyst and measure its catalytic reaction rate. Clearly, *TOF* of the catalyst has a quasi volcanic relationship with different Cu/Ni ratios in Fig. 5b and Table S4. Among them, $NiCu_3$-N-C DAC has the largest *TOF* of 3.64 s^{-1}, which is 4.2 times of Ni-N-C SAC and 3.3 times of Cu-N-C SAC. The *TOF* value measures the reaction rate on the catalyst, focusing on the "active site", eliminating the impact of specific surface area of the carrier, substrate diffusion, etc. As a supplement for more comprehensively evaluating the inherent activity of each catalyst, the electrochemical specific surface area (*ECSA*) was calculated. As shown in Fig. S5, current responses at different scanning speeds on the $NiCu_3$-N-C DAC, as well as that on the controls. Δj has a good linear correlation with Δv, where the slope obtained is twice the electrical double-layer capacitance (Fig. 5c). The calculated *ECSA* of $NiCu_3$-N-C DAC reaches 237 cm^2, which is significantly better than its control catalysts.

Furthermore, EIS was used to elaborate the electrochemical reaction kinetics of AOR. According to the fitting analysis of the equivalent circuit, the high frequency region and low frequency region in Nyquist

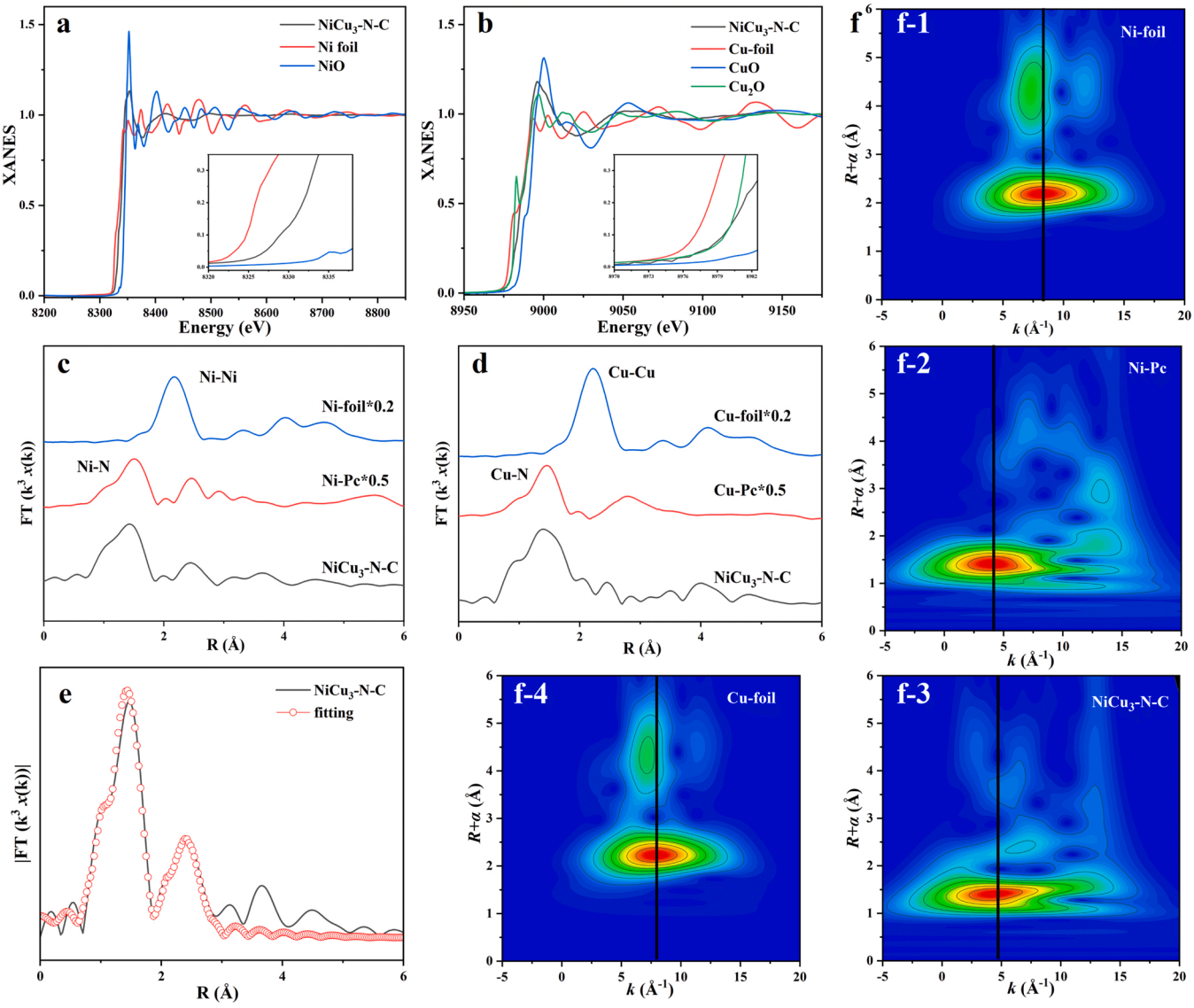

Fig. 4. All for $NiCu_3$-N-C DAC: (a) Ni and (b) Cu K-edge XANES spectra; (c) Ni and (d) Cu K-edge FT-EXAFS curves; (e) the fitting curves of Ni K-edge EXAFS in R-space; (f) WT plots of $NiCu_3$-N-C, Ni-Pc, Ni-foil, and Cu-foil.

diagram are governed by charge transfer and substance diffusion, separately (Fig. 5d). The fitting results exhibit that Cu-N-C SAC has the largest resistance of charge transfer (R_{ct}, 0.62 Ω) and Warburg slope (k, 4.77), illustrating that although the charge-transfer rate is slow, the substance diffusion rate is fast. Relatively, Ni-N-C SAC has a smaller R_{ct} (0.16 Ω) and a faster charge transfer rate. The electronic interaction between nickel-copper diatoms in $NiCu_x$-N-C DACs is influenced by the Cu/Ni ratio. The experimental results indicated that $NiCu_3$-N-C DAC achieved a minimal R_{ct} of 0.01 Ω and k of 4.13 when this ratio is 3/1, allowing faster charge transfer and substance diffusion to be maintained at the catalyst/electrolyte interface. In short, good electronic coupling effect occurs between bimetallic sites in $NiCu_3$-N-C DAC, ameliorating the internal electronic structure, which greatly expedites the AOR kinetics to gain an extraordinary catalytic activity.

3.3. Removal performance of ammonia-nitrogen

Using the catalyst of $NiCu_3$-N-C DAC, the effect of different initial concentrations of ammonia (C_0: 1400, 700 and 350 mg/L) on the removal performance for synthetic ammonia-nitrogen wastewater was investigated under a specified voltage of 1.50 V vs. RHE. From the comparison of LSV curves obtained with different C_0 in Fig. 6a, it was found that the higher the C_0, the larger the current response assembled on the catalyst surface. Subsequently, the results of the ammonia-nitrogen removal experiments lasting for 5 h exhibited that the degradation rate of NH_4^+-N was evidently accelerated when the C_0 was raised from 350 to 700 mg/L (Fig. 6b and S6a). Under the same operation time of 5 h, their removal efficiency of NH_4^+-N reached 98.74% for C_0 = 350 mg/L and 99.16% for C_0 = 700 mg/L respectively, where the removed amount has nearly doubled with an increase from 345.59 mg N to 694.12 mg N (Fig. 6c). When C_0 increased to 1400 mg/L, the degradation rate was not further accelerated and only 55.38% of removal efficiency was attained. This attributes to the finite active sites and the oversaturation of ammonia-nitrogen that can be treated per unit time. Note that the higher the C_0, the more NO_3^- and NO_2^- were also generated as seen in Figs. S6b-c. As a result, the best N_2 selectivity (97.87%) was obtained when the C_0 was 700 mg/L (Fig. 6d). To better evaluate the effect on the removal performance of NH_4^+-N, the Faradaic efficiency (*FE*) and Energy Consumption (*EC*) of the reaction were calculated (Fig. 6e-f). Clearly, the highest *FE* of 84.5% and the smallest *EC* of 0.08 kW h/kg N were achieved while the C_0 was 700 mg/L. Taken together, it points out that the catalyst can be utilized at its optimum

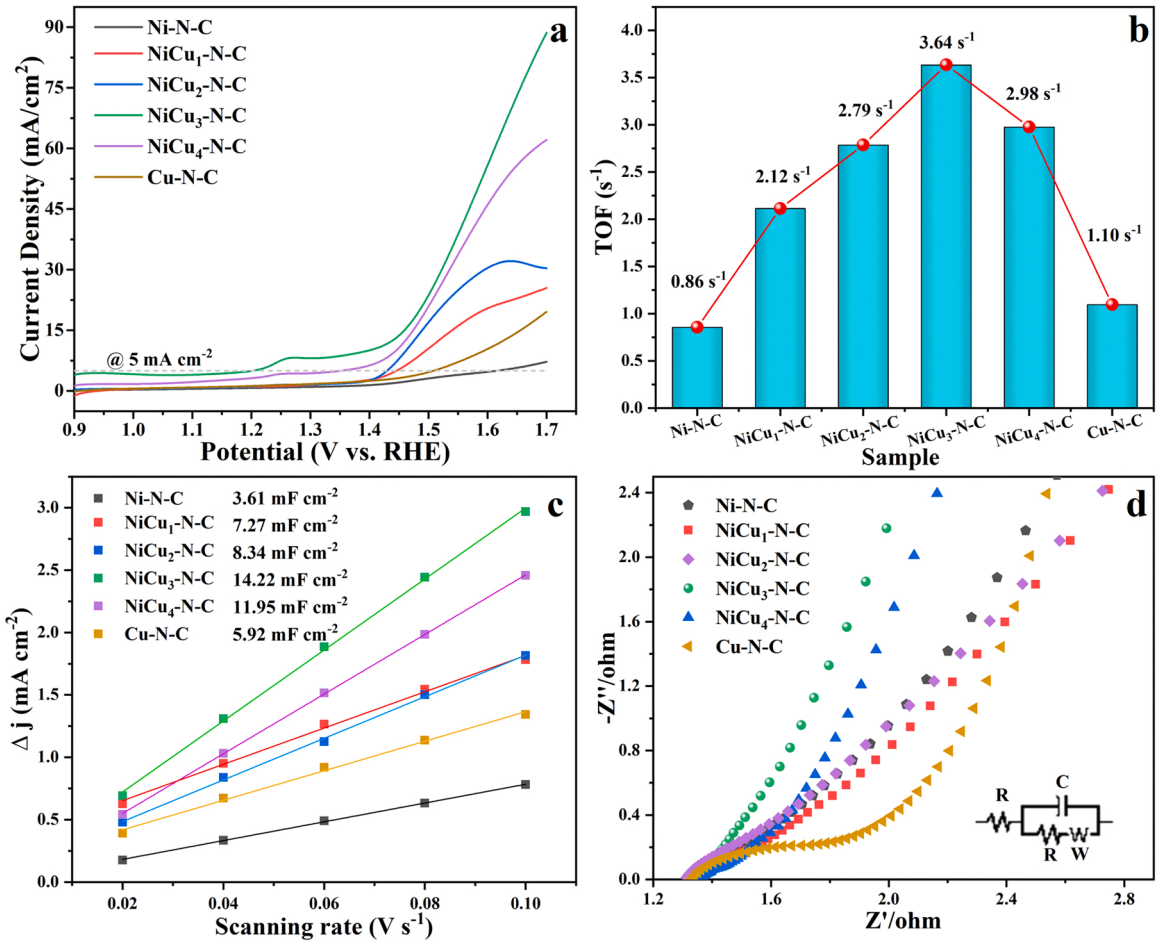

Fig. 5. The comparison of electrochemical performances collected on the surface of $NiCu_3$-N-C and its control catalysts. (a) LSV curves in 1 M NaOH + 0.2 M NH_4Cl; (b) Turnover Frequency (*TOF*); (c) Curve of Δj versus scanning rate; (d) Nyquist plots obtained by EIS measurement.

concentration for ammonia-nitrogen removal to the maximum extent. In addition, multi-cycle ammonia nitrogen removal experiments (5 h per cycle)were carried out at the optimal treatment concentration. As shown in Fig. S9, the removal efficiency of NH_4^+-N did not decrease significantly in the experiment results of three cycles, which was still more than 97.6%, manifesting the stability of $NiCu_3$-N-C DAC.

Then, the effect of operating potential on the removal performance was investigated for a synthetic wastewater with the 700 mg/L of NH_4^+-N. As shown in Fig. 7a-b, the higher the operating potential, the higher the current response and the faster the degradation rate of NH_4^+-N. Also, the removal efficiency of NH_4^+-N raised from 66.32% to 99.76%, while that of TN raised from 67.04% to 94.15% during the same degradation time (Fig. 7e). Surprisingly, there is only a slight increase in generation of NO_3^- and NO_2^- with the potential (Fig. S7c-d). This is because, unlike nanoscale catalysts with diverse site expression, the coordinated homogeneous diatomic sites of the $NiCu_3$-N-C DAC can drive the AOR towards the desired G-M mechanism. It can be clearly seen that the N_2 selectivity exceeds 95% for all potential conditions (Fig. 7f), highlighting the weak effect of the operating potential on the N_2 selectivity. Considering practical applications, a lower operating potential was acquired while ensuring a high removal efficiency of NH_4^+-N, meaning higher economic benefits. Hence, the operating potential of 1.50 V is the optimum solution for AOR process of the catalyst. As a complement, the same experiments were performed for the control catalysts, such as Ni-N-C, $NiCu_1$-N-C, $NiCu_2$-N-C, $NiCu_4$-N-C and Cu-N-C (Fig. S7a-d). Explicitly, it was observed that the $NiCu_3$-N-C DAC exhibited optimal LSV activity, fastest degradation rate and the maximum removal efficiency of NH_4^+-N (98.32%) and TN (95.89%). This stems from the existence of electronic interactions between the Ni/Cu diatomic sites and the highly atomically dispersed active centers, thus greatly heightening the potential catalytic capacity of AOR.

3.4. Real application

Accordingly, the experiment using the real wastewater with 616 mg/L NH_4^+-N was conducted at 1.50 V vs. RHE for 6 h to examine the practical performance of $NiCu_3$-N-C DAC. Also, the similar experments of the nano-scale Ni_1Cu_3-S-T/CP and $Ni_1Cu_1Co_{0.5}$-S-T/CP catalysts attained in previous works, were applied as controls under the same operating conditions[25,26]. Obviously, the $NiCu_3$-N-C DAC initiates AOR earlier than the control nano-scale catalysts, accompanied by a onset potential difference of nearly 0.4 V vs. RHE @ 1 mA/cm^2 (Fig. 8a). The variation curves of current density with the degradation time was shown in Fig. 8b, and then the changes of different nitrogen species concentrations in wastewater with degradation time were aqcuired, including the indexes of NH_4^+-N, NO_2^--N, NO_3^--N and TN (Fig. 8c-f). The degradation rate of NH_4^+-N is faster on the $NiCu_3$-N-C DAC than that on nano-scale catalysts, owing to more rapid charge transfer and substance transport at the catalyst/electrolyte interface at the atomic level. As such, the removal efficiency of NH_4^+-N on the $NiCu_3$-N-C DAC after electrolysis for 6 h was as high as 99.52%, but that on Ni_1Cu_3-S-T/CP and $Ni_1Cu_1Co_{0.5}$-S-T/CP only were 91.43% and 86.19%, respectively (Fig. 8g).

Emphasizedly, the initial concentrations of NO_3^--N of 150 mg/L and NO_2^--N of 305 mg/L was coexisted in the real wastewater. Interestingly, the trends of NO_2^--N concentration in the $NiCu_3$-N-C DAC system and

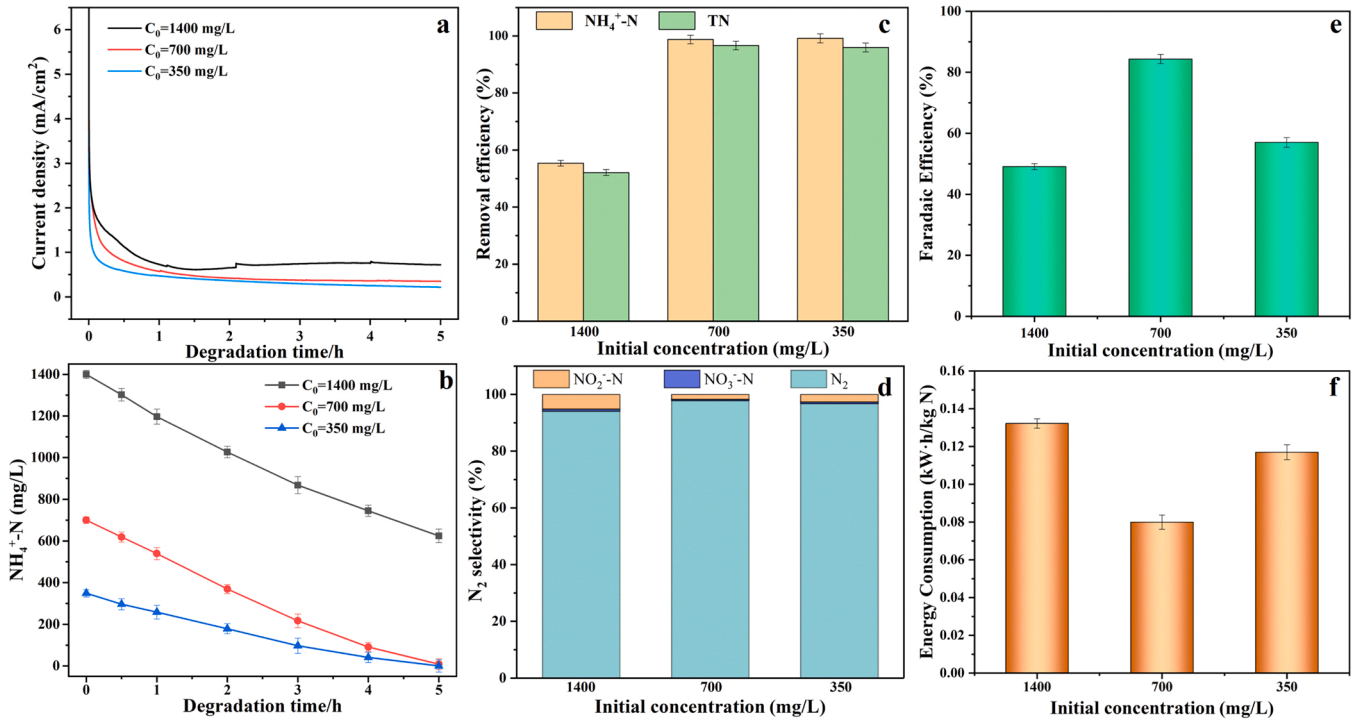

Fig. 6. The effect of various initial concentrations on the removal performance of NH_4^+-N, collected by $NiCu_3$-N-C DAC. Comparisons of (a) Variation curves of current density with degradation time; (b) Degradation of NH_4^+-N; (c) Removal efficiency of NH_4^+-N and TN; (d) N_2 selectivity; (e) Faradaic efficiency (*FE*); (f) Energy Consumption (*EC*).

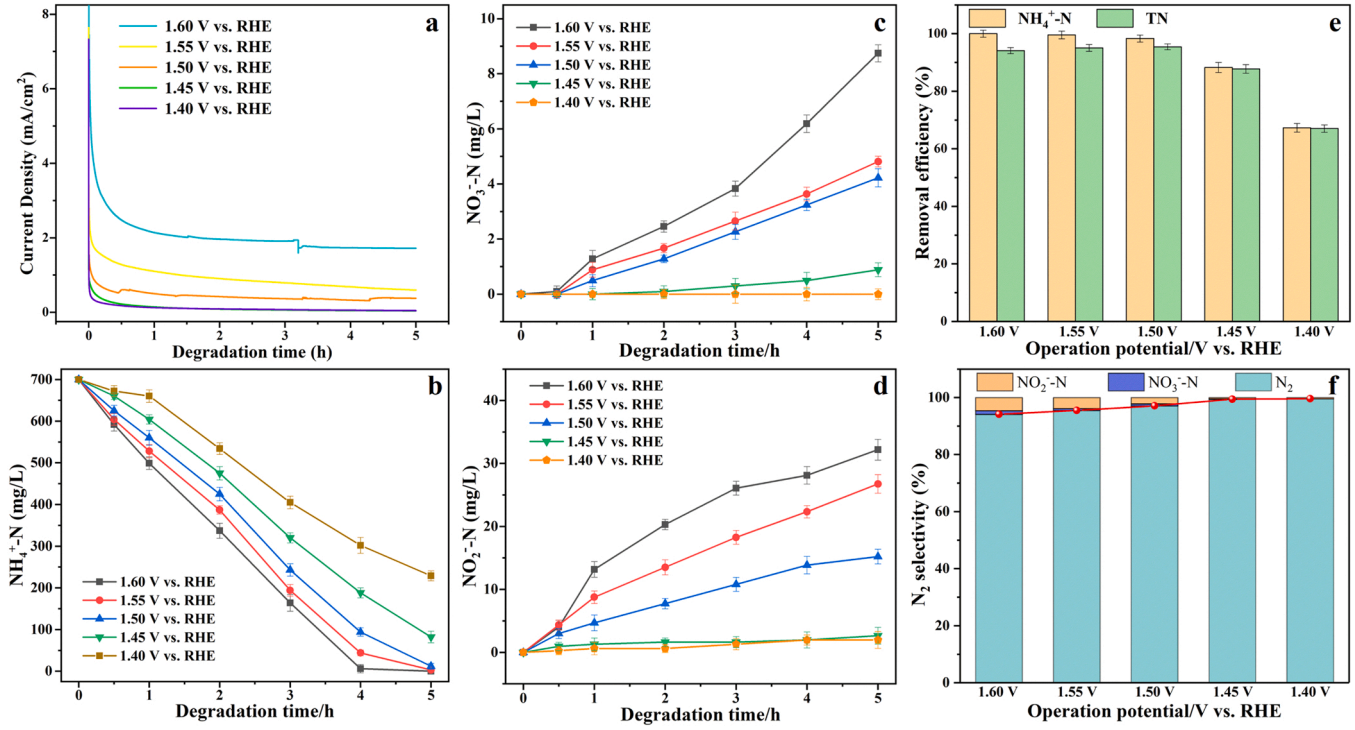

Fig. 7. The effect of different potential conditions on the removal performance of NH_4^+-N, collected by $NiCu_3$-N-C DAC. (a) Variation curves of current density with degradation time in the synthetic wastewater of 700 mg/L NH_4^+; Variation curves of (b) NH_4^+-N, (c) NO_3^--N, (d) NO_2^--N concentration with degradation time; (e) Removal efficiency of NH_4^+-N and TN; (f) N_2 selectivity.

nanoscale catalyst systems are widely different. The removal efficiency of NO_2^--N in the $NiCu_3$-N-C DAC system was 13.66%, much higher than that of only 2.74% in the nano-scale $Ni_1Cu_1Co_{0.5}$-S-T/CP system. Worse still, the NO_2^--N concentration in the electrolytic system of Ni_1Cu_3-S-T/CP did not decrease, but increased by 14.88%. This is because almost no side reactions occur on the anode side in the $NiCu_3$-N-C DAC system, while they occur in the systems of nano-scale catalysts. Besides, it is reasonable to deduce that part of pristine nitrate is converted to nitrite

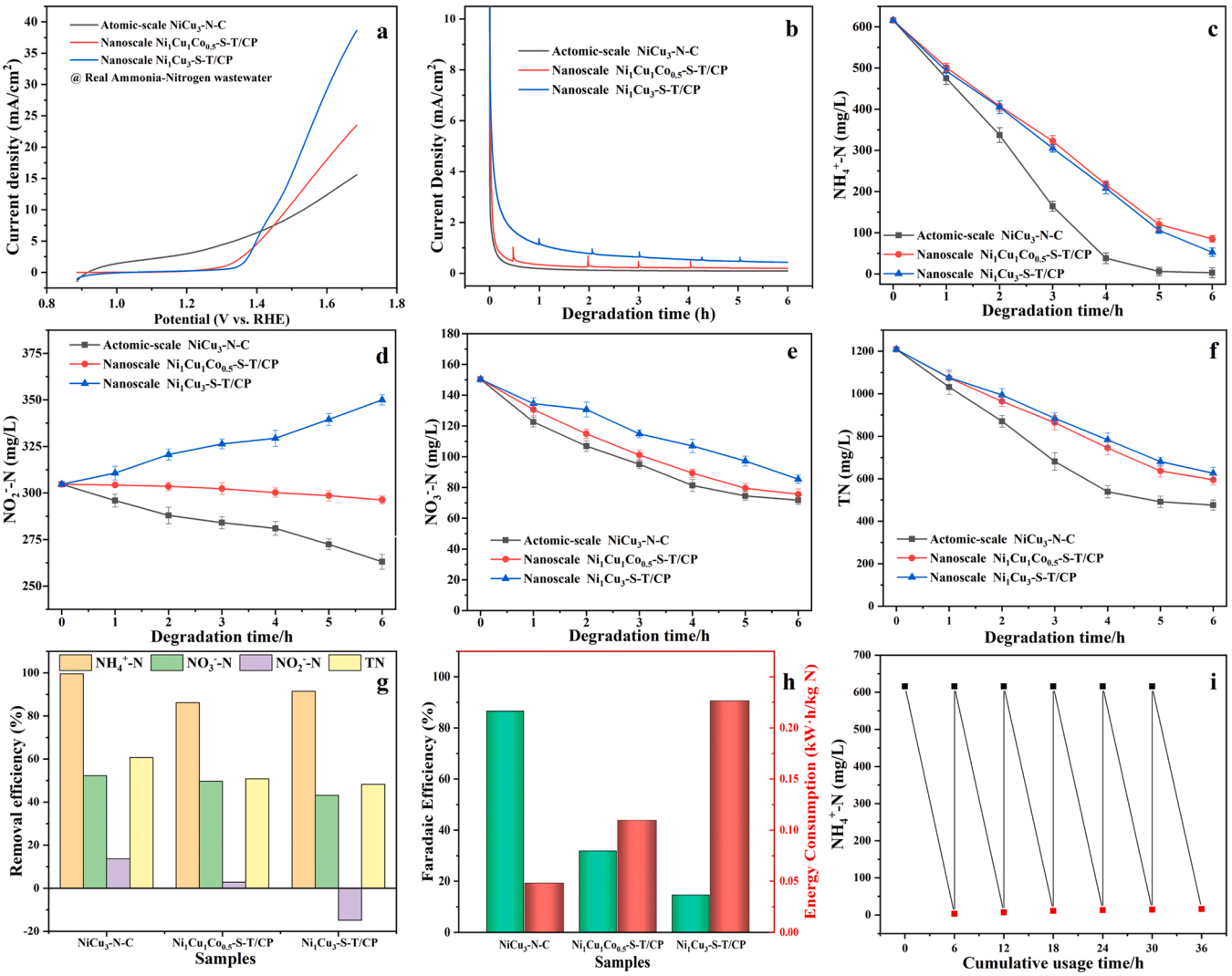

Fig. 8. Comparison of the ammonia-nitrogen removal performance on the surface of $NiCu_3$-N-C DAC, $Ni_1Cu_1Co_{0.5}$-S-T/CP and Ni_1Cu_3-S-T/CP nanoscale catalysts. (a) LSV curves; (b) Variation curves of current density with degradation time; Variation curves of (c) NH_4^+-N, (d) NO_2^--N, (e) NO_3^--N and (f) TN concentration with degradation time; (g) Removal efficiency of nitrogen species, noted: negative value of removal efficiency represents an increase of NO_2^--N in the electrolytic system of Ni_1Cu_3-S-T/CP; (h) Faradaic efficiency and Energy consumption; (i) Changes of NH_4^+-N concentration during multi-cycle ammonia-nitrogen removal experiments.

and part is directly reduced to N_2 in the cathodic electrochemical reduction process. As a consequence, the $NiCu_3$-N-C DAC system can achieve a higher removal efficiency of 60.64% for TN than in the systems of nano-scale catalysts (48.19% for Ni_1Cu_3-S-T/CP, 50.78% for $Ni_1Cu_1Co_{0.5}$-S-T/CP).

Furthermore, as shown in Fig. 8h, $NiCu_3$-N-C DAC gained higher *FE* (86.60%) than the nano-scale catalysts with 14.66% of *FE* (Ni_1Cu_3-S-T/CP) and 31.79% ($Ni_1Cu_1Co_{0.5}$-S-T/CP). Meanwhile, less *EC* of 0.05 kW h/kg N was also acquired in the $NiCu_3$-N-C DAC system, compared with that in the systems of nano-scale catalysts (0.23 kW h/kg N for Ni_1Cu_3-S-T/CP, 0.12 kW h/kg N for $Ni_1Cu_1Co_{0.5}$-S-T/CP). This highlights the preeminent catalytic performance of the $NiCu_3$-N-C DAC, which can allow to achieve better removal efficiency at a lower cost. It further points to the importance of improving the atom utilisation efficiency, as well as obtaining a precise and singular active expression. Finally, multi-cycles of ammonia-nitrogen removal experiments (per cycle for 6 h) were run to further assess the durability of the $NiCu_3$-N-C DAC (Fig. 8i). The removal efficiency of NH_4^+- N barely shows a decline with the increase of usage times. Thus, $NiCu_3$-N-C DAC still holds considerable potential in the field of direct electrochemical oxidation treatment for ammonia-nitrogen wastewater.

Generally, nanoscale metal catalysts are composed of a variety of nanoparticles and sub-nanoclusters with varying particle size, which have multiple active sites such as different crystalline planes and vertices. This means that their catalytic activity is expressed in an ensemble diversity, making it difficult to ensure that all $*NH_3$ forms hydrazine intermediates ($*N_2H_{x+y}$) after the first step of dehydrogenation. Consequently, the AOR pathway on the surfaces of Ni_1Cu_3-S-T/CP and $Ni_1Cu_1Co_{0.5}$-S-T/CP catalysts likely tends to follow an O-S

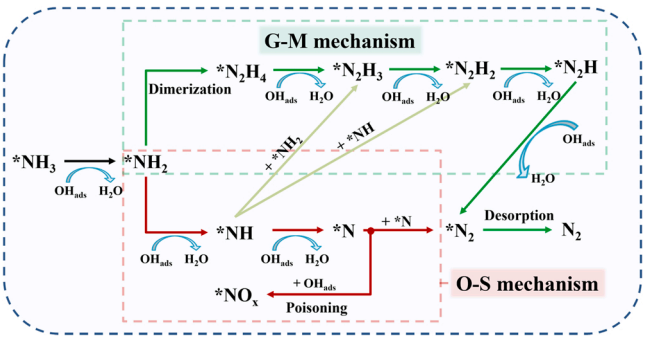

Fig. 9. Schematic description of AOR mechanism.

mechanism as shown in Fig. 9: *NH_3 gradually dehydrogenates to *N species, then dimerizes to N_2[54]. During this process, *N is highly susceptible to further peroxidation to produce toxic by-products, e.g., NO_2^- and NO_3^-. In contrast, atomic scale catalysts have a low coordination number and a special unsaturated coordination environment, in which the highly dispersed distribution of active metal atoms confers a highly homogeneous structure of the active sites. As a result, they exhibit an extremely high single product selectivity for multi-electron step reactions. Naturally, the AOR pathway on the atomic scale catalyst surface follows the G-M mechanism as shown in Fig. 9: *NH_3 dehydrogenates to *NH_2, *NH_x and *NH_y dimerize to generate *N_2H_{x+y}, and then dehydrogenate in one step to form N_2[30]. The $NiCu_3$-N-C DAC has coordinated Ni/Cu atoms, where the bimetallic electron interactions well optimize the internal electronic structure to ameliorate its adsorption capacity to intermediates. It is reasonable to infer that the adjacent diatomic sites allow two molecules of NH_3 to be absorbed onto the surface of Ni and Cu atoms, respectively. Then, a strongly stable N-N bond in hydrazine intermediates (*N_2H_{x+y}) is formed after the removal of a proton, followed by further dehydrogenation to form N_2. This well unveils the underlying mechanism of the high N_2 selectivity in the catalytic AOR process by the $NiCu_3$-N-C DAC. Of course, it is worthwhile to reveal the structural properties such as bond length/bond energy/bond angle at the level of molecular structure of catalysts, then diving and dissecting deeper reaction mechanism for further research.

4. Conclusions

In this work, $NiCu_3$-N-C DAC anchored in nitrogen-doped carbon has been synthesised via a facile solid-phase pyrolysis method. HAADF-STEM and XAFS characterizations confirmed the diatomic sites structure and their highly dispersed distribution characteristics, while revealing the local coordination environment of Ni-N_4/Cu-N_4 groups. The specific restricted micro-environment allows the catalyst to high-selectively promote the direct electrochemical oxidation of ammonia to N_2, resulting in efficient treatment of ammonia-nitrogen wastewater, accompanied by resourcefulness and harmlessness of the products. Results demonstrate that $NiCu_3$-N-C DAC with Ni-N_4/Cu-N_4 groups has a high intrinstic activity for AOR, with a higher *TOF* of 3.64 s^{-1} compared to that for Ni-N-C (0.86 s^{-1}) and Cu-N-C (1.10 s^{-1}) at 1.50 V vs. RHE. Obviously, the electronic coupling effect between the adjacent metal sites of Ni-N_4 and Cu-N_4 optimizes the internal electronic structure of the catalyst and balances the adsorption freedom degree of various nitrogen intermediates, thus acquiring a faster proton-electron transfer rate. After the ammonia-nitrogen removal experiment for 5 h, it exhibited a NH_4^+-N removal efficiency of 99.52% with a high N_2 selectivity of 97.87% in synthetic wastewater. Naturally, it achieved 99.52% of NH_4^+-N removal efficiency and 86.60% of *FE* after that for 6 h in real wastewater. Overall, the Ni-N_4/Cu-N_4 diatomic sites in $NiCu_3$-N-C DAC can achieve the desired pathway for AOR, giving important insights for the development of green and economic technologies. Also, it provides a outstanding example for the rational design of functionally coordinated DACs, which advances the application of electrochemical oxidation technology in ammonia-nitrogen wastewater treatment.

CRediT authorship contribution statement

Huimin Zhang: Conceptualization, Resources, Funding acquisition, Writing – review & editing, Supervision. **Hailong Wang:** Methodology, Investigation, Validation, Data curation, Formal analysis, Visualization, Writing – original draft, Writing – review & editing. **Luanqi Zhou**: Data curation, Formal analysis, Visualization. **Qiming Li**: Data curation, Formal analysis. **Xu Yang**: Supervision, Writing – review & editing. **Yifei Wang**: Supervision, Project administration. **Meng Zhang**: Supervision, Project administration. **Zucheng Wu**: Supervision, Project administration.

Declaration of Competing Interest

The authors declare that they have no known competing financial interests or personal relationships that could have appeared to influence the work reported in this paper.

Data Availability

The authors do not have permission to share data.

Acknowledgments

This work was supported by the National Natural Science Foundation of China (No. 51768019) and Project of Education Department of Jiangxi Province (GJJ2200608).

Appendix A. Supporting information

Supplementary data associated with this article can be found in the online version at doi:10.1016/j.apcatb.2023.122544.

References

[1] U.B. Shahid, K. Siddharth, M. Shao, Electrifying the nitrogen cycle: an electrochemical endeavor, Curr. Opin. Electrochem. 30 (2021).
[2] V. Rosca, M. Duca, M.T. de Groot, M.T.M. Koper, Nitrogen cycle electrocatalysis, Chem. Rev. 109 (2009) 2209–2244.
[3] L. Qin, M. Gao, M. Zhang, L. Feng, Q. Liu, G. Zhang, Application of encapsulated algae into MBR for high-ammonia nitrogen wastewater treatment and biofouling control, Water Res 187 (2020), 116430.
[4] H. Chang, M. Lu, Y. Zhu, Z. Zhang, Z. Zhou, Y. Liang, R.D. Vidic, Consideration of potential technologies for ammonia removal and recovery from produced water, Environ. Sci. Technol. 56 (2022) 3305–3308.
[5] Q. Zhang, X. Chen, Z. Zhang, W. Luo, H. Wu, L. Zhang, X. Zhang, T. Zhao, Performance and microbial ecology of a novel moving bed biofilm reactor process inoculated with heterotrophic nitrification-aerobic denitrification bacteria for high ammonia nitrogen wastewater treatment, Bioresour. Technol. 315 (2020), 123813.
[6] J. Ji, Y. Peng, B. Wang, X. Li, Q. Zhang, Synergistic partial-denitrification, anammox, and in-situ fermentation (SPDAF) process for advanced nitrogen removal from domestic and nitrate-containing wastewater, Environ. Sci. Technol. 54 (2020) 3702–3713.
[7] W. Verstraete, S. Philips, Nitrification-denitrification processes and technologies in new contexts, Environ. Pollut. 102 (1998) 717–726.
[8] A.T. Ukwuani, W. Tao, Developing a vacuum thermal stripping - acid absorption process for ammonia recovery from anaerobic digester effluent, Water Res 106 (2016) 108–115.
[9] Y. Li, X. Li, H.S. Pillai, J. Lattimer, N. Mohd Adli, S. Karakalos, M. Chen, L. Guo, H. Xu, J. Yang, D. Su, H. Xin, G. Wu, Ternary PtIrNi catalysts for efficient electrochemical ammonia oxidation, ACS Catal. 10 (2020) 3945–3957.
[10] M. Zhang, H. Li, X. Duan, P. Zou, G. Jeerh, B. Sun, S. Chen, J. Humphreys, M. Walker, K. Xie, S. Tao, An efficient symmetric electrolyzer based on bifunctional perovskite catalyst for ammonia electrolysis, Adv. Sci. (Weinh.) 8 (2021), e2101299.
[11] M. Zhang, P. Zou, G. Jeerh, B. Sun, M. Walker, S. Tao, Oxygen Vacancy-Rich $La_{0.5}Sr_{1.5}Ni_{0.9}Cu_{0.1}O_{4-\delta}$ as a High-Performance Bifunctional Catalyst for Symmetric Ammonia Electrolyzer, Adv. Funct. Mater. 32 (2022).
[12] P. Mandal, M.K. Yadav, A.K. Gupta, B.K. Dubey, Chlorine mediated indirect electro-oxidation of ammonia using non-active PbO_2 anode: influencing parameters and mechanism identification, Sep. Purif. Technol. 247 (2020).
[13] P. Saha, J. Wang, Y. Zhou, L. Carlucci, A.W. Jeremiasse, H.H.M. Rijnaarts, H. Bruning, Effect of electrolyte composition on electrochemical oxidation: Active sulfate formation, benzotriazole degradation, and chlorinated by-products distribution, Environ. Res. 211 (2022), 113057.
[14] K. Nagita, Y. Yuhara, K. Fujii, Y. Katayama, M. Nakayama, Ni- and Cu-co-intercalated layered manganese oxide for highly efficient electro-oxidation of ammonia selective to nitrogen, ACS Appl. Mater. Interfaces 13 (2021) 28098–28107.
[15] C. Zhong, W.B. Hu, Y.F. Cheng, Recent advances in electrocatalysts for electro-oxidation of ammonia, J. Mater. Chem. A 1 (2013) 3216–3238.
[16] Mt Bezdek, S. Guo, P. Chirik, Coordination-induced weakening of ammonia, water, and hydrazine X-H bonds in a molybdenum complex, Science 354 (2016) 730–733.
[17] T.L. Lomocso, E.A. Baranova, Electrochemical oxidation of ammonia on carbon-supported bi-metallic PtM (M=Ir, Pd, SnO_x) nanoparticles, Electrochim. Acta 56 (2011) 8551–8558.
[18] J.R. Barbosa, M.N. Leon, C.M. Fernandes, R.M. Antoniassi, O.C. Alves, E.A. Ponzio, J.C.M. Silva, $PtSnO_2$/C and Pt/C with preferential (100) orientation: High active electrocatalysts for ammonia electro-oxidation reaction, Appl. Catal. B: Environ. 264 (2020), 118458.

[19] R. Wang, H. Liu, K. Zhang, G. Zhang, H. Lan, J. Qu, Ni(II)/Ni(III) redox couple endows Ni foam-supported Ni_2P with excellent capability for direct ammonia oxidation, Chem. Eng. J. 404 (2021), 126795.

[20] J. Huang, Z. Chen, J. Cai, Y. Jin, T. Wang, J. Wang, Activating copper oxide for stable electrocatalytic ammonia oxidation reaction via in-situ introducing oxygen vacancies, Nano Res. 15 (2022) 5987–5994.

[21] W. Xu, D. Du, R. Lan, J. Humphreys, D.N. Miller, M. Walker, Z. Wu, J.T.S. Irvine, S. Tao, Electrodeposited NiCu bimetal on carbon paper as stable non-noble anode for efficient electrooxidation of ammonia, Appl. Catal. B: Environ. 237 (2018) 1101–1109.

[22] W. Xu, R. Lan, D. Du, J. Humphreys, M. Walker, Z. Wu, H. Wang, S. Tao, Directly growing hierarchical nickel-copper hydroxide nanowires on carbon fibre cloth for efficient electrooxidation of ammonia, Appl. Catal. B: Environ. 218 (2017) 470–479.

[23] H.M. Zhang, Y.F. Wang, Y.H. Kw, A direct ammonia microfluidic fuel cell using NiCu nanoparticles supported on carbon nanotubes as an electrocatalystt, ChemSusChem 11 (2018) 2889–2897.

[24] H. Zhang, W. Chen, H. Wang, X. Tong, Y. Wang, X. Yang, Z. Wu, Z. Liu, A core-shell NiCu@NiCuOOH 3D electrode induced by surface electrochemical reconstruction for the ammonia oxidation reaction, Int. J. Hydrog. Energy 47 (2022) 16080–16091.

[25] H. Zhang, H. Wang, X. Tong, L. Zhou, X. Yang, Y. Wang, M. Zhang, Z. Wu, Sulfur induced surface reconfiguration of Ni_1Cu_3-S-T/CP anode for high-efficiency ammonia electro-oxidation, Chem. Eng. J. 452 (2023), 139582.

[26] H. Wang, X. Tong, L. Zhou, Y. Wang, L. Liao, S. Ouyang, H. Zhang, Unique three-dimensional nanoflower-like NiCu electrodes constructed by Co, S co-doping for efficient ammonia oxidation reaction, Sep. Purif. Technol. 303 (2022), 122293.

[27] M. Zhu, Y. Yang, S. Xi, C. Diao, Z. Yu, W.S.V. Lee, J. Xue, Deciphering NH_3 adsorption kinetics in ternary Ni-Cu-Fe oxyhydroxide toward efficient ammonia oxidation reaction, Small 17 (2021), e2005616.

[28] C. Tang, H.S. Wang, H.F. Wang, Q. Zhang, G.L. Tian, J.Q. Nie, F. Wei, Spatially confined hybridization of nanometer-sized NiFe hydroxides into nitrogen-doped graphene frameworks leading to superior oxygen evolution reactivity, Adv. Mater. 27 (2015) 4516–4522.

[29] C. Guo, J. Ran, A. Vasileff, S.-Z. Qiao, Rational design of electrocatalysts and photo (electro)catalysts for nitrogen reduction to ammonia (NH_3) under ambient conditions, Energy Environ. Sci. 11 (2018) 45–56.

[30] J. Hou, Y. Cheng, H. Pan, P. Kang, CuSn double-metal hydroxides for direct electrochemical ammonia oxidation to dinitrogen, ChemElectroChem 9 (2022).

[31] Y.-J. Shih, C.-H. Hsu, Kinetics and highly selective N_2 conversion of direct electrochemical ammonia oxidation in an undivided cell using NiCo oxide nanoparticle as the anode and metallic Cu/Ni foam as the cathode, Chem. Eng. J. 409 (2021).

[32] D. Zhou, X. Li, H. Shang, F. Qin, W. Chen, Atomic regulation of metal–organic framework derived carbon-based single-atom catalysts for the electrochemical CO_2 reduction reaction, J. Mater. Chem. A 9 (2021) 23382–23418.

[33] M. Li, H. Wang, W. Luo, P.C. Sherrell, J. Chen, J. Yang, Heterogeneous single-atom catalysts for electrochemical CO_2 reduction reaction, Adv. Mater. 32 (2020), e2001848.

[34] A. Majumdar, P. Dutta, A. Sikdar, H. Lee, D. Ghosh, S. Jha, S. Tripathi, Y. Oh, U. Maiti, Impact of atomic rearrangement and single atom stabilization on $MoSe_2$@ $NiCo_2Se_4$ heterostructure catalyst for efficient overall water splitting, Small 18 (2022), 2200622.

[35] H. Yang, Y. Liu, Y. Luo, S. Lu, B. Su, J. Ma, Achieving high activity and selectivity of nitrogen reduction via Fe–N_3 coordination on iron single-atom electrocatalysts at ambient conditions, ACS Sustain. Chem. Eng. 8 (2020) 12809–12816.

[36] C. Ren, Q. Jiang, W. Lin, Y. Zhang, S. Huang, K. Ding, Density functional theory study of single-atom V, Nb, and Ta catalysts on graphene and carbon nitride for selective nitrogen reduction, ACS Appl. Nano Mater. 3 (2020) 5149–5159.

[37] K. Qi, M. Chhowalla, D. Voiry, Single atom is not alone: Metal–support interactions in single-atom catalysis, Mater. Today 40 (2020) 173–192.

[38] W.-H. Li, J. Yang, H. Jing, J. Zhang, Y. Wang, J. Li, J. Zhao, D. Wang, Y. Li, Creating high regioselectivity by electronic metal-support interaction of a single-atomic-site catalyst, J. Am. Chem. Soc. (2021).

[39] D. Zhao, Z. Zhuang, X. Cao, C. Zhang, Q. Peng, C. Chen, Y. Li, Atomic site electrocatalysts for water splitting, oxygen reduction and selective oxidation, Chem. Soc. Rev. 49 (2020) 2215–2264.

[40] W. Wan, Y. Zhao, S. Wei, C.A. Triana, J. Li, A. Arcifa, C.S. Allen, R. Cao, G. R. Patzke, Mechanistic insight into the active centers of single/dual-atom Ni/Fe-based oxygen electrocatalysts, Nat. Commun. 12 (2021) 5589.

[41] W. Orellana, Catalytic properties of transition Metal–N4 moieties in graphene for the oxygen reduction reaction: evidence of spin-dependent mechanisms, J. Phys. Chem. C. 117 (2013) 9812–9818.

[42] S. Jin, Z. Hao, K. Zhang, Z. Yan, J. Chen, Advances and challenges for the electrochemical reduction of CO_2 to CO: from fundamentals to industrialization, Angew. Chem. Int. Ed. Engl. 60 (2021) 20627–20648.

[43] A. Pedersen, J. Barrio, A. Li, R. Jervis, J. Dan, M.M. Titirici, I. Stephens, Dual-Metal Atom Electrocatalysts: Theory, Synthesis, Characterization, and Applications, Advanced Energy Materials.

[44] W. Ren, X. Tan, W. Yang, C. Jia, S. Xu, K. Wang, S.C. Smith, C. Zhao, Isolated diatomic Ni-Fe metal-nitrogen sites for synergistic electroreduction of CO_2, Angew. Chem. Int Ed. Engl. 58 (2019) 6972–6976.

[45] L. Li, K. Yuan, Y. Chen, Breaking the scaling relationship limit: from single-atom to dual-atom catalysts, Acc. Mater. Res. 3 (2022) 584–596.

[46] J. Hao, Z. Zhuang, J. Hao, C. Wang, S. Lu, F. Duan, F. Xu, M. Du, H. Zhu, Interatomic electronegativity offset dictates selectivity when catalyzing the CO_2 reduction reaction, Adv. Energy Mater. 12 (2022).

[47] D. Yao, C. Tang, X. Zhi, B. Johannessen, A. Slattery, S. Chern, S.Z. Qiao, Inter-metal interaction with a threshold effect in NiCu dual-atom catalysts for CO_2 electroreduction, Adv. Mater. (2022), e2209386.

[48] M. Liu, N. Li, S. Cao, X. Wang, X. Lu, L. Kong, Y. Xu, X.H. Bu, A. Pre-Constrained, MetaL Twins" Strategy to Prepare Efficient Dual-metal-atom Catalysts for Cooperative Oxygen Electrocatalysis, Adv. Mater. 34 (2022), e2107421.

[49] Z. Pei, X.F. Lu, H. Zhang, Y. Li, D. Luan, X.W. Lou, Highly efficient electrocatalytic oxygen evolution over atomically dispersed synergistic Ni/Co dual sites, Angew. Chem. Int. Ed. 61 (2022).

[50] D. Liu, Y. Zhao, C. Wu, W. Xu, S. Xi, M. Chen, L. Yang, Y. Zhou, Q. He, X. Li, B. Ge, L. Song, J. Jiang, Q. Yan, Triggering electronic coupling between neighboring hetero-diatomic metal sites promotes hydrogen evolution reaction kinetics, Nano Energy 98 (2022), 107296.

[51] T. Ding, X. Liu, Z. Tao, T. Liu, T. Chen, W. Zhang, X. Shen, D. Liu, S. Wang, B. Pang, D. Wu, L. Cao, L. Wang, T. Liu, Y. Li, H. Sheng, M. Zhu, T. Yao, Atomically precise dinuclear site active toward electrocatalytic CO_2 reduction, J. Am. Chem. Soc. 143 (2021) 11317–11324.

[52] Q. Wang, B. Jin, M. Hu, C. Jia, X. Li, E. Sharman, J. Jiang, N-doped graphene-supported diatomic Ni–Fe catalyst for synergistic oxidation of CO, J. Phys. Chem. C. 125 (2021) 5616–5622.

[53] J. Fu, J. Dong, R. Si, K. Sun, J. Zhang, M. Li, N. Yu, B. Zhang, M.G. Humphrey, Q. Fu, J. Huang, Synergistic effects for enhanced catalysis in a dual single-atom catalyst, ACS Catal. 11 (2021) 1952–1961.

[54] K. Yang, J. Liu, B. Yang, Mechanism and active species in NH_3 dehydrogenation under an electrochemical environment: an ab initio molecular dynamics study, ACS Catal. 11 (2021) 4310–4318.